The peeling behavior of thin films with finite bending stiffness and the implications on gecko adhesion

Roger A. Sauer [1]

Aachen Institute for Advanced Study in Computational Engineering Science (AICES), RWTH Aachen University, Templergaben 55, 52056 Aachen, Germany

Published[2] in *The Journal of Adhesion*, DOI: 10.1080/00218464.2011.596084
Submitted on 8 June 2010, Revised on 18 October 2010, Accepted on 29 October 2010

Abstract

Analytical thin film peeling models, like the Kendall model (Kendall, 1975), are formulated under restricting assumptions concerning the strip geometry, the material behavior, the peeling kinematics and the contact behavior. Recently, such models have been applied to study the peeling of gecko spatulae, although the gecko spatula is significantly different from an idealized thin film. Especially the bending stiffness of the spatula has a strong influence on the peeling force which is neglected in the Kendall model. This is demonstrated here by several detailed finite element computations, based on a geometrically exact deformation model and a refined contact description for van der Waals adhesion. Therefore, the peeling of an elastic strip is considered and the influence of the bending stiffness is studied. It is shown that the adhesion induces a bending moment within the strip that can become very large and must therefore be accounted for in the strip formulation and evaluation of the work of adhesion. Further, the implications on the computation of the peeling behavior of gecko spatulae are discussed. It is observed that the spatula geometry lies in the range where the peeling work attains a maximum.

keywords: van der Waals adhesion, thin film peeling, computational contact mechanics, nonlinear beam formulation, finite element method

1 Introduction

The adhesion and peeling properties of thin films are important to many applications, like paint and coating technology, adhesive tapes, cell adhesion and gecko adhesion. One of the most widely used models for the mechanical description of peeling is the analytical peeling model of Kendall (1975). The Kendall model, which accounts for the axial stiffness of the film but neglects the bending and shear stiffness, has been extended by many researchers to account for root rotation (Williams, 1993), non-linear material behavior (Williams and Kauzlarich, 2005; Molinari and Ravichandran, 2008), shear and bending stiffness (Li et al., 2004; Thouless and Yang, 2008) and pre-tension (Chen et al., 2009). To reflect current research, a special issue on peel testing has appeared recently (Moore (Ed.), 2008).
In recent studies, peeling models have been applied to the gecko spatula (Huber et al., 2005; Tian et al., 2006; Pesika et al., 2007; Chen et al., 2009; Peng et al., 2010). These studies, however, consider the Kendall regime, where the bending stiffness is negligible. Also missing are the influences of the section rotation and the shear in the peeling zone, which affect the

[1]email: sauer@aices.rwth-aachen.de

computation of the peeling forces and the peeling work. These influences lead to strongly non-linear peeling models that need to be solved by numerical methods like the finite element method. Detailed 2D and 3D finite element models, however, tend to become very costly, especially for peeling computations where sharp stresses need to be resolved at the peeling front (Sauer, 2011). It therefore becomes advantageous to develop efficient numerical models that are based on reduced kinematics, like beam theories.
This paper assesses the influence of the bending stiffness on thin film peeling and argues that detailed models need to be used for films with finite bending stiffness, especially in the example of the gecko spatula. Three main purposes are served:

1. to show that a bending moment is induced within the film due to adhesion and to discuss its influence on the work of adhesion; therefore the notion of the partial work of adhesion is introduced;

2. to discuss the influence of finite bending stiffness on thin film peeling by examining the film deformation, the peeling force and the peeling work; and

3. to discuss the implications on gecko adhesion.

As a framework we consider the adhesion formulation of Sauer and Li (2007b,a), which is based on the Lennard-Jones potential and computational contact mechanics (Wriggers, 2006). This formulation offers several advantages over other methods like cohesive zone models: It is based on a variational principle, it is suitable for van der Waals adhesion and allows to combine common contact descriptions used at different length scales into a unified framework (Sauer and Li, 2007b, 2008). The formulation also bears resemblance with cohesive zone models used in fracture mechanics. For the results presented here, the adhesion formulation is incorporated into a nonlinear finite element approach based on non-linear beam theory.
The remainder of this paper is structured as follows: Sec. 2 shows that certain special cases, like peeling by pure bending, can be solved analytically. Sec. 3 discusses the work of adhesion, which is a central parameter for peeling, and shows how it can be computed accurately for thin films and strips. Due to adhesion, a distributed force and bending moment are induced within the film. In Sec. 4, the formulation is used within a nonlinear finite element approach to analyze the peeling behavior of thin films with finite bending stiffness. Sec. 5 concludes this paper.

2 Work balance of the peeling film

This section applies the balance of work to the peeling of an elastic film and shows that two special cases can be described analytically. Quasi-static and plane strain conditions are considered. In order to peel an adhering film from an adhesive substrate work must be provided. This external work is converted into the internal energy stored inside the elastic deformation and the contact energy required to separate the adhering bodies. In incremental form we thus have

$$\mathrm{d}\Pi_{\mathrm{ext}} = \mathrm{d}\Pi_{\mathrm{int}} + \mathrm{d}\Pi_{\mathrm{c}} \ . \tag{1}$$

This result essentially corresponds to the theorem of expended work, which is a consequence of the balance of linear momentum (Gurtin, 1981). The three incremental work contributions are discussed in the following three sections. We therefore, consider an elastic strip with length L, height h and width b adhering to a substrate along the bottom surface $L \times b$. The substrate is considered perfectly flat.

2.1 External work

Suppose that the strip is loaded at one end by an applied force $\boldsymbol{F}$ and bending moment M. Given an infinitesimal displacement $\mathrm{d}\boldsymbol{u}$ and rotation $\mathrm{d}\theta$, the external work changes by

$$\mathrm{d}\Pi_{\mathrm{ext}} = \boldsymbol{F} \cdot \mathrm{d}\boldsymbol{u} + M\,\mathrm{d}\theta \ . \tag{2}$$

Both $\boldsymbol{F}$ and M are supposed to act within the plane formed by the strip axis and substrate normal (see Fig. 1). The force can be decomposed into the components along these directions, denoted by F_1 and F_2, so that

$$\mathrm{d}\Pi_{\mathrm{ext}} = F_1\,\mathrm{d}u_1 + F_2\,\mathrm{d}u_2 + M\,\mathrm{d}\theta \ . \tag{3}$$

2.2 Internal energy

For an elastic body $\mathcal{B}$, the internal elastic energy corresponds to the work done by the internal forces and elastic deformations. These can be characterized by the stress tensor $\boldsymbol{\sigma}$ and the strain tensor $\boldsymbol{\varepsilon} = \frac{1}{2}(\nabla\boldsymbol{u} + (\nabla\boldsymbol{u})^T)$. The incremental increase of the internal energy, due to an incremental increase of the deformation is thus given by

$$\mathrm{d}\Pi_{\mathrm{int}} = \int_{\mathcal{B}} \boldsymbol{\sigma} : \mathrm{d}\boldsymbol{\varepsilon}\,\mathrm{d}V \ . \tag{4}$$

According to the Euler-Bernoulli beam theory[3] the deformation of the strip is characterized by the axial strain ε and the bending curvature κ, while the internal forces are characterized by the axial force $N = EA\varepsilon$ and bending moment $M = EI\kappa$, so that expression (4) becomes

$$\mathrm{d}\Pi_{\mathrm{int}} = \int_0^L \left(EA\,\varepsilon\,\mathrm{d}\varepsilon + EI\,\kappa\,\mathrm{d}\kappa\right)\mathrm{d}L \ . \tag{5}$$

Here EA and EI denote the axial stiffness and bending stiffness, that are obtained from Young's modulus E, the cross section area $A = bh$ and the second moment of area $I = bh^3/12$ of the rectangular cross-section of the strip. Considering a homogeneous strip with constant EA and EI, the integration over the strain interval $[0, \varepsilon]$ and the curvature interval $[0, \kappa]$ yields the internal energy

$$\mathrm{d}\Pi_{\mathrm{int}} = \tfrac{1}{2}EA\,\varepsilon^2\,\mathrm{d}L + \tfrac{1}{2}EI\,\kappa^2\,\mathrm{d}L \ . \tag{6}$$

within the strip segment $\mathrm{d}L$. During peeling of the strip, the initially undeformed length $\mathrm{d}L$ is newly stretched and bend, so that eq. (6) describes the change in the internal energy of the strip.

2.3 The contact energy

The contact energy corresponds to the work done by the contact traction T_{c} over the contact surface. When two adhering surfaces are separated, the contact energy can also be formulated in terms of the work of adhesion w_{adh}, which is defined as the energy per unit area necessary to fully separate two adhering bodies (Israelachvili, 1991). It is often considered as a material parameter. During peeling, as the peeling surface increases by the area $\mathrm{d}A_{\mathrm{c}}$, the contact energy therefore increases by

$$\mathrm{d}\Pi_{\mathrm{c}} = w_{\mathrm{adh}}\,\mathrm{d}A_{\mathrm{c}} \ . \tag{7}$$

A discussion on the accurate computation of w_{adh} is given in Sec. 3.

[3]The Euler-Bernoulli beam theory assumes linear elastic material behavior and neglects the work done by the shear forces

2.4 Applications

In some cases it is possible to exploit the equations above analytically. Two fundamental peeling examples, shown in Fig. 1, are discussed in the following.

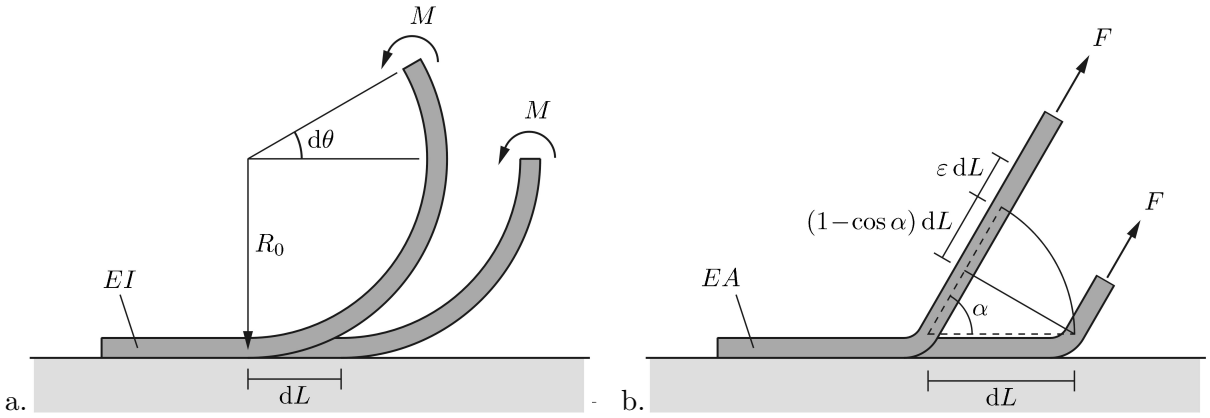

Figure 1: Fundamental peeling examples: a. peeling by pure bending; b. peeling by pure stretching.

2.4.1 Peeling by pure bending

We first consider the peeling of a rectangular strip by applying a rotation to the end of the strip. In this case the strip is subjected to pure bending between the peeling front and the right end as is shown in Fig. 1.a. The bending radius is denoted by R_0, so that $\kappa = R_0^{-1}$. If an additional rotation increment $\mathrm{d}\theta$ is applied at the end, the peeling zone advances by $\mathrm{d}L = R_0\mathrm{d}\theta$, and we have $\mathrm{d}\Pi_{\mathrm{int}} = \frac{1}{2}EI\kappa\,\mathrm{d}\theta$, $\mathrm{d}\Pi_{\mathrm{ext}} = M\,\mathrm{d}\theta$ and $\mathrm{d}\Pi_{\mathrm{c}} = w_{\mathrm{adh}}bR_0\,\mathrm{d}\theta$ according to the equations above. Using the relation $M = EI\kappa$ with $I = bh^3/12$, eq. (1) thus yields the expression

$$\frac{M}{Ebh^2} = \sqrt{\frac{w_{\mathrm{adh}}}{6Eh}}\,, \tag{8}$$

for the bending moment M, and the relation

$$\frac{R_0}{h} = \sqrt{\frac{Eh}{24w_{\mathrm{adh}}}}\,, \tag{9}$$

for the bending radius R_0. If w_{adh} increases by a factor of γ, the bending moment will increase by $\sqrt{\gamma}$ and the bending radius will decrease by $\sqrt{\gamma}$. For a gecko spatula pad with $E = 2\,\mathrm{GPa}$, $h = 10\,\mathrm{nm}$ and $w_{\mathrm{adh}} = 30.66\,\mathrm{mJ/m^2}$ (Sauer, 2009), we have $w_{\mathrm{adh}}/(Eh) = 1.533\cdot 10^{-3}$ and therefore $M/b = 3.197\,\mathrm{nN}$ and $R_0 = 52.13\,\mathrm{nm}$.[4] These values come very close to the result found from a detailed nonlinear finite element analysis, which accounts for the complex 2D deformation field at the peeling front. This has been considered in Sauer (2011), where we have found $M/b = 3.283\,\mathrm{nN}$.[5] According to that computation, the average bending radius is 52.67 nm, which shows that the detailed FE result behaves slightly stiffer.
Concluding, we note that expression (8) can only be used if the bending radius R_0 is constant,

[4] w_{adh} is computed from eq. (18) using $A_{\mathrm{H}} = 10^{-19}\,\mathrm{J}$ and $r_0 = 0.4\,\mathrm{nm}$.

[5] In Sauer (2011) we have reported $M/b = 1.6414\,EL_0^2$ which is equal to $M/b = 3.283\,\mathrm{nN}$ since $E = 2\,\mathrm{GPa}$ and $L_0 = 1\,\mathrm{nm}$ there.

which is not the case if the peeling forces are long range, or if an external force, instead of a moment, is applied, as is seen from the results in Sec. 4.

2.4.2 Peeling by pure stretching

As a second example, we consider the peeling by an applied force as is shown in Fig. 1.b. During peeling, the amount of bending does not change so that the bending energy does not contribute to the energy change described by eq. (6). But as Sec. 3 shows, the strip curvature in the peeling zone can affect the adhesion energy w_{adh}. According to Fig. 1.b, we now have $\mathrm{d}\Pi_{\mathrm{int}} = \frac{1}{2}EA\,\varepsilon^2\,\mathrm{d}L$, $\mathrm{d}\Pi_{\mathrm{c}} = w_{\mathrm{adh}}\,b\,\mathrm{d}L$ and $\mathrm{d}\Pi_{\mathrm{ext}} = F[(1-\cos\alpha)+\varepsilon]\mathrm{d}L$. Using the relation $F = N = EA\,\varepsilon$, eq. (1) then gives

$$\frac{F^2}{2Ehb^2} + \frac{F}{b}(1-\cos\alpha) = w_{\mathrm{adh}}\ , \tag{10}$$

which is the well known result according to Kendall (1975). The positive root of this equation is given by

$$\frac{F}{EA} = \sqrt{(1-\cos\alpha)^2 + 2\frac{w_{\mathrm{adh}}}{Eh}} - (1-\cos\alpha)\ . \tag{11}$$

To assess the influence of w_{adh} on F, we consider the reference energy $w_{\mathrm{adh},\infty} = 1.533\cdot 10^{-3}Eh$ associated with gecko adhesion (see Sec. 2.4.1) and compare the force $F(w_{\mathrm{adh}} = \gamma w_{\mathrm{adh},\infty})$ to the reference case $F_{\mathrm{ref}} = F(w_{\mathrm{adh}} = w_{\mathrm{adh},\infty})$. This is shown in Fig. 2 for the values $\gamma = 1/2$, $\gamma = 1$ and $\gamma = 2$. Fig. 2.b shows that the influence of w_{adh} is most prominent for large α, where

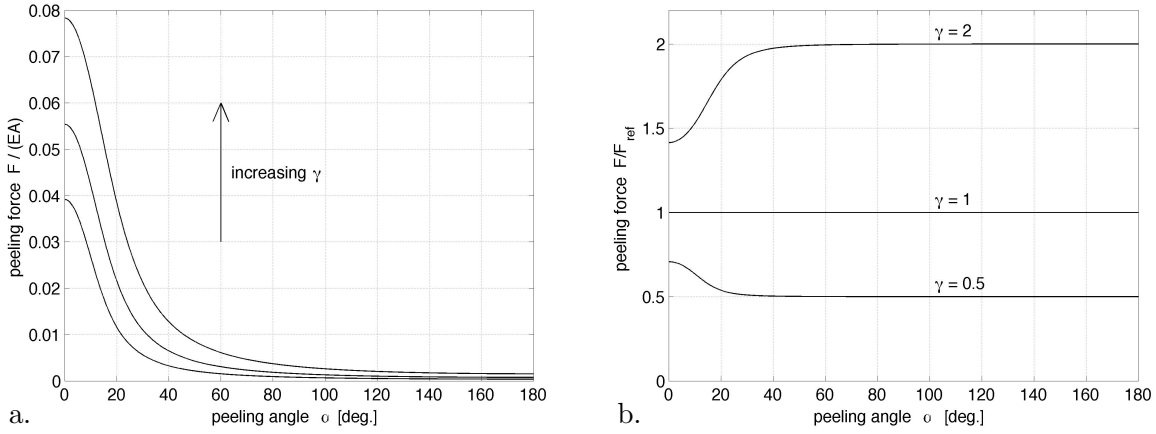

Figure 2: Peeling force $F(\alpha, w_{\mathrm{adh}})$ according to eq. (11) (Kendall, 1975) for the adhesion parameters $w_{\mathrm{adh}} = \gamma w_{\mathrm{adh},\infty}$ with $\gamma = 1/2$, $\gamma = 1$ and $\gamma = 2$: a. normalization of F by EA; b. normalization of F by F_{ref}.

F changes by γ, whereas F only changes by $\sqrt{\gamma}$ for $\alpha = 0$.[6]
It is important to note that the Kendall solution neglects the bending stiffness of the strip since it assumes that F is parallel to the strip axis. It is shown in Sec. 4 that the bending stiffness is quite high for the gecko spatula and thus the Kendall model does not apply since it underestimates the peeling force substantially. One should also note that the Kendall result only provides the force during peeling but gives no information on the force build-up and the snap-off behavior. In general, these can only be obtained from numerical approaches like the

[6] It can be formally shown that $F/F_{\mathrm{ref}} = \sqrt{\gamma}$ for $\alpha = 0$ and $F/F_{\mathrm{ref}} = \gamma$ for $w_{\mathrm{adh},\infty}/(Eh) \ll (1-\cos\alpha)$.

finite element method considered in Sec. 4. These methods require an accurate evaluation of the contact energy, as is discussed in the following section.

3 The work of adhesion for films and strips

In this section we reexamine the work of adhesion, adapt the concept to peeling films and assess the influence of the film height and the bending curvature at the peeling front.
The results of the preceding section are based on the work of adhesion which is introduced as a material constant. It is defined as the surface energy required to fully separate two adhering bodies. This approach works well for the two preceding examples, since the global energy of the strip is considered. But the concept cannot be used in the following two cases: If the the strip is not fully peeled off the substrate and, more generally, if a finite element formulation is used. The reason for the second case is that the local energies of the individual elements need to be evaluated. These are considerably lower than w_{adh} for those elements that have only partially separated. We therefore need to find an expression of the work of adhesion for partial separation, which we denote 'partial work of adhesion'. For thin films, this depends on the film height and the bending curvature of the strip during peeling.
Let us first consider that the surfaces of the two bodies remain parallel during separation and describe the separation by the coordinate r. The work of adhesion for a separation from the equilibrium distance $r = r_{\mathrm{eq}}$ up to the arbitrary distance $r = r_d$ is then given by

$$w_{\mathrm{adh}}(r_d) = -\int_{r_{\mathrm{eq}}}^{r_d} T_{\mathrm{c}}\,\mathrm{d}r_{\mathrm{s}}\ , \tag{12}$$

where T_{c} denotes the distance dependant surface traction acting on the separated surface located at $r = r_{\mathrm{s}}$. In the remainder of this discussion, we consider the Lennard-Jones potential in order to define this traction. However, any other traction-separation law, like the Xu-Needleman model (Xu and Needleman, 1994) or Coulomb interaction, can be used within the following framework. For the Lennard-Jones potential, which is suitable to describe van-der-Waals adhesion, T_{c} follows from the integration of the body force[7]

$$B_{\mathrm{c}}(r) = \frac{A_{\mathrm{H}}}{2\pi r_0^4}\left[\frac{1}{5}\left(\frac{r_0}{r}\right)^{10} - \left(\frac{r_0}{r}\right)^{4}\right] \tag{13}$$

over the height of the strip. Here A_{H} denotes Hamaker's constant and r_0 denotes the equilibrium distance of the Lennard-Jones potential. Denoting the upper and lower boundaries of the film by r_1 and r_2 we thus have

$$T_{\mathrm{c}} = \int_{r_1}^{r_2} B_{\mathrm{c}}(r)\,\mathrm{d}r\ , \tag{14}$$

i.e.

$$T_{\mathrm{c}} = T(r_1) - T(r_2)\ , \tag{15}$$

with

$$T(r) = \frac{A_{\mathrm{H}}}{2\pi r_0^3}\left[\frac{1}{45}\left(\frac{r_0}{r}\right)^{9} - \frac{1}{3}\left(\frac{r_0}{r}\right)^{3}\right]\ , \tag{16}$$

according to eq. (13). The equilibrium spacing between the adhering surfaces, r_{eq}, is the spacing where $T_{\mathrm{c}}(r_{\mathrm{s}} = r_{\mathrm{eq}}) = 0$. If the film height is sufficiently large[8],

$$r_{\mathrm{eq}} = \sqrt[6]{1/15}\,r_0\ . \tag{17}$$

[7] This expression is obtained by integrating the Lennard-Jones force over the neighboring body which is approximated by a flat half-space (Sauer and Wriggers, 2009).

[8] For $h > 3.5\,\mathrm{nm}$ and $r_0 = 0.4\,\mathrm{nm}$ the contribution from boundary r_2 becomes less than 10^{-3} times the maximum adhesion value $T_{\max} = \sqrt{5}A_{\mathrm{H}}/(9\pi r_0^3)$. Thus $T_{\mathrm{c}} \approx T(r_1)$ and r_{eq} follows from $T = 0$.

For full separation ($r_d = \infty$), one then finds from eq. (12)

$$w_{\mathrm{adh},\infty} = \sqrt[3]{15}\frac{A_{\mathrm{H}}}{16\pi r_0^2} \ . \tag{18}$$

During peeling, the contact surface curves away from the substrate. This behavior does not affect $w_{\mathrm{adh},\infty}$, since it makes no difference on which path $r_d = \infty$ is reached. For finite r_d, however, the surface curvature affects the partial work of adhesion substantially and one cannot use expression (12). Three effects occur: 1. an apparent increase of the film density, 2. an additional bending moment and 3. the shear deformation of the film. The last effect is only significant for shear flexible films, which are not discussed in detail here. The first two effects are illustrated in Fig. 3 and are discussed in the following. In order to draw general conclusions, it is important to account for the deformation of the film and note that the body force B_{c} acts on the volume element $\mathrm{d}v_1$ of the deformed strip $\mathcal{B}_1$. As it is more convenient to integrate the body forces over the undeformed strip configuration $\mathcal{B}_{01}$, the body forces have to be formulated with respect to the undeformed volume element $\mathrm{d}V_1$. This is the case of the expression given in eq. (13) (Sauer and Wriggers, 2009).

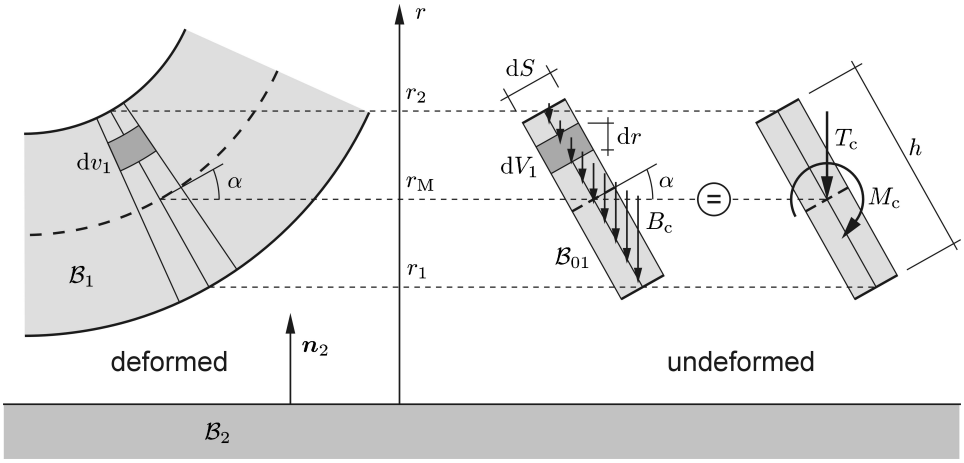

Figure 3: Cross-sectional film force T_{c} and bending moment M_{c} induced by adhesion. These act on the deformed configuration of the film, denoted $\mathcal{B}_1$, but can be conveniently computed by integration over the undeformed configuration of the film, denoted $\mathcal{B}_{01}$.

1. Due to the bending of the film, segment $\mathrm{d}S$ is inclined by the angle α, so that the undeformed volume element $\mathrm{d}V_1$ can be written as

$$\mathrm{d}V_1 = \frac{b\,\mathrm{d}r\,\mathrm{d}S}{\cos\alpha} \ . \tag{19}$$

The $(\cos\alpha)^{-1}$ term corresponds to an apparent increase of the density along direction r. The surface traction introduced in eq. (14)–(16) thus changes to

$$\tilde{T}_{\mathrm{c}} = \frac{T_{\mathrm{c}}}{\cos\alpha} \ . \tag{20}$$

2. Due to the inclination of the film, the adhesion forces induce a bending moment, M_{c}, as is shown in Fig. 3. It is caused by the eccentricity

$$e = (r_{\mathrm{M}} - r)\tan\alpha \tag{21}$$

of the body force B_c. Here, r_M denotes the location of the center axis of the film. The integration across the film height then defines the sectional bending moment as

$$M_c = \int_{r_1}^{r_2} (r_M - r) \tan\alpha \, \frac{B_c(r)}{\cos\alpha} \, dr \ . \tag{22}$$

According to eqs. (13) and (14), this integration yields

$$M_c = \left(r_M \, T_c - r_0 \, T_c^*\right) \frac{\tan\alpha}{\cos\alpha} \ , \tag{23}$$

with

$$T_c^* = \int_{r_1}^{r_2} r \, B_c \, dr = T^*(r_1) - T^*(r_2) \ , \tag{24}$$

and

$$T^*(r) = \frac{A_H}{2\pi r_0^3} \left[\frac{1}{40} \left(\frac{r_0}{r}\right)^8 - \frac{1}{2} \left(\frac{r_0}{r}\right)^2 \right] . \tag{25}$$

According to Fig. 3, the boundaries of the film are given by

$$r_1(\alpha) = r_M - \frac{h}{2} \cos\alpha \ , \quad r_2(\alpha) = r_M + \frac{h}{2} \cos\alpha \ . \tag{26}$$

The work of adhesion now follows as the work done by the traction T_c and the moment M_c from the equilibrium configuration of the cross-section, at position $r = r_{eq}$ and inclination $\alpha = 0$, to the current configuration of the section, at $r = r_d$ and $\alpha = \alpha_d$, i.e.

$$w_{adh}(r_d, \alpha_d) = -\int_{r_{eq}}^{r_d} \frac{T_c}{\cos\alpha} \, dr_M - \int_0^{\alpha_d} M_c \, d\alpha \ . \tag{27}$$

The two terms appearing in eq. (27) are denoted by $w_{adh,T}$ and $w_{adh,M}$ in the following. The second term does not appear in the original formulation given in eq. (12). Depending on the film height h and the local bending curvature κ of the film, this part can become very large, as is illustrated by the following figures. For this illustration, we consider the special case where the bent film axis lies on a circle with radius R_0, i.e.

$$r_M(\alpha) = r_{eq} + R_0(1 - \cos\alpha) + h/2 \ , \tag{28}$$

so that the work of adhesion becomes

$$w_{adh}(\alpha_d) = -\int_0^{\alpha_d} \frac{T_c}{\cos\alpha} \, R_0 \sin\alpha \, d\alpha - \int_0^{\alpha_d} M_c \, d\alpha \ . \tag{29}$$

which can be easily evaluated numerically. Fig. 4 shows the dependency of the two terms $w_{adh,T}$ and $w_{adh,M}$, normalized by $w_0 = w_{adh,\infty}$, on the film curvature radius R_0 for five different values of the film height h. For large ratios h/R_0, the contribution of $w_{adh,M}$ becomes very large: If $h/R_0 > 0.1$, contribution $w_{adh,M}$ accounts for more than 5% of w_{adh}. Surprisingly, this is even the case for large bending radii R_0, so that we cannot use approximation (12) even then. As the figure shows, this approximation can only be used for small h/R_0. Here, we have considered ratios up to the physical limit $h/R_0 = 2$. For the range of parameters considered in the figure, the sum $w_{adh} = w_{adh,T} + w_{adh,M}$ is equal to $w_{adh,\infty}$. In all cases the peeling angle is set to $\alpha_d = \pi/2$.

Fig. 5 shows the dependency of $w_{adh,T}$ and $w_{adh,M}$ on the film height h for six different values of the film curvature radius R_0. Again, $\alpha_d = \pi/2$ and $h/R_0 \leq 2$ are considered. For very small values of h, below 1 nm, the total work of adhesion $w_{adh} = w_{adh,T} + w_{adh,M}$ is significantly lower

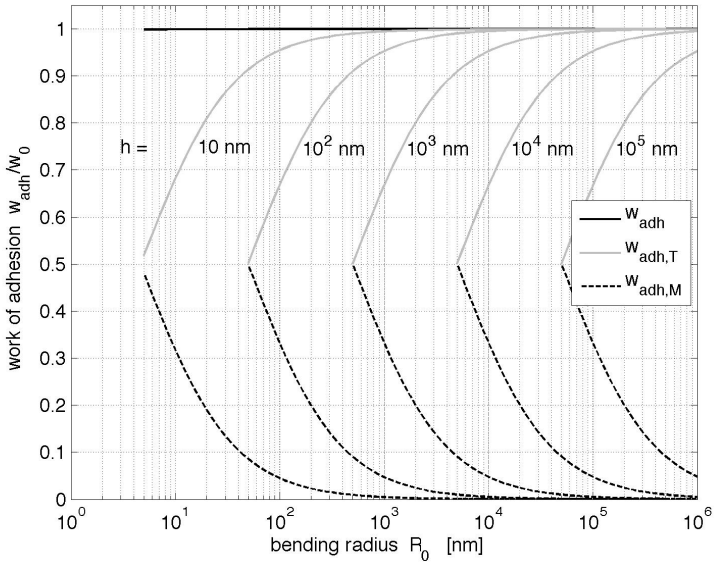

Figure 4: Influence of the bending radius R_0 of the peeling film on the contributions of the work of adhesion $w_{\mathrm{adh,T}}$ and $w_{\mathrm{adh,M}}$ for five different values of the film height h. If $h/R_0 > 0.1$ contribution $w_{\mathrm{adh,M}}$ accounts for more than 5% of w_{adh}.

than $w_{\mathrm{adh},\infty}$, due to effect of the upper boundary on integration (14).[9] Only for large h do $w_{\mathrm{adh,T}}$ and $w_{\mathrm{adh,M}}$ add up to $w_{\mathrm{adh},\infty}$. But note that when h/R_0 is large, approximation (12) cannot be used since $w_{\mathrm{adh,M}}$ becomes large.
Finally, Fig. 6 shows the influence of α_d, the third and last free parameter affecting w_{adh} according to eq. (29). Here, we have considered $h = 10\,\mathrm{nm}$ and $R_0 = 50\,\mathrm{nm}$. It can be seen that the work of adhesion is only saturated (i.e. $w_{\mathrm{adh}} \approx w_{\mathrm{adh},\infty}$) beyond $\alpha_d = 20°$.
The three figures illustrate that it is important to evaluate the work of adhesion according to eq. (27) instead of using eq. (12). This is especially important for large values of h/R_0, which are typically attained for soft films with strong adhesion, like the gecko spatula. For the spatula, we have $h/R_0 \approx 0.2$ as is noted in Sec. 2.4.1.

4 Accurate peeling behavior of an elastic film

This section discusses the influence of the bending stiffness on the peeling behavior of the elastic film and compares this case to the special cases for zero and infinite bending stiffness.[10] These computations are based on a finite beam element formulation of the Timoshenko (i.e. shear flexible) beam theory, that is geometrically exact, i.e. the non-linear beam kinematics of large deformations are captured exactly (Wriggers, 2008). Details of this formulation will be reported in a future publication. As a test case, a strip with height $h = 10\,\mathrm{nm}$ and length $L = 200\,\mathrm{nm}$ is considered in the following, which resembles the dimensions of the spatula pad that is located at the tip of the gecko foot hairs (Tian et al., 2006). Plane strain deformation is considered,

[9] Note that for very small h, the equilibrium spacing is not equal to eq. (17) and must be recomputed from $T_c(r_{\mathrm{eq}}) = 0$.
[10] Note that we also have finite bending stiffness in the analytical model of Sec. 2.4.1, however, in that model special kinematics are considered which are not general and do not apply to combined bending, extension and shear as is considered here.

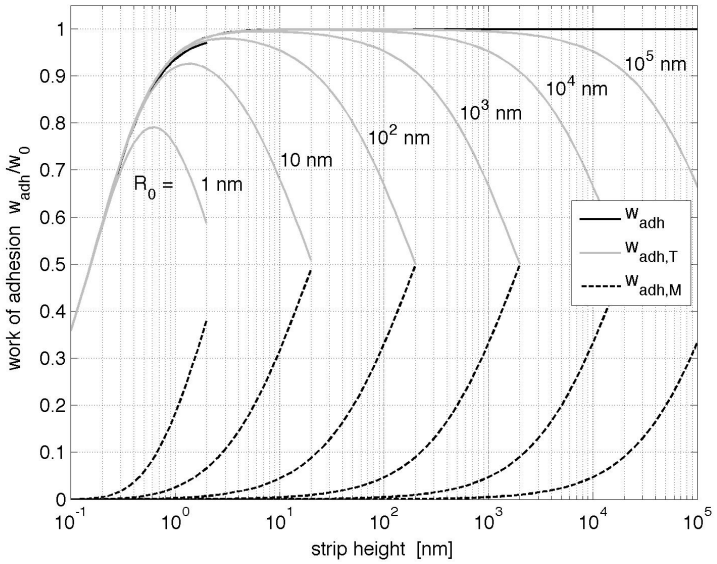

Figure 5: Influence of the film height h on the contributions of the work of adhesion $w_{\mathrm{adh,T}}$ and $w_{\mathrm{adh,M}}$ for six different values of the bending radius R_0.

such that the strip width b does not need to be specified. The strip material is modeled linear elastically with Young's modulus E and Poisson's ratio ν, which is taken as $\nu = 0.2$ for the following examples. The strip is pulled upward by applying a vertical displacement u at the right boundary ($x = L$). During peeling, the strip remains free to rotate at this boundary. The left boundary (at $x = 0$) remains unconstrained. Adhesive, frictionless contact is considered along 75% of the bottom surface of the strip (from $x = 0$ to $x = L_{\mathrm{c}} = 150\,\mathrm{nm}$). The adhesive contact forces are derived from the Lennard Jones potential (see Sec. 3) giving the line load T_{c} and moment M_{c} acting on the beam (see eqs. (15) and (23)). Before discussing the finite element results the following two special cases are examined.

1. Peeling force for $EI = 0$: The case for zero bending stiffness corresponds to the Kendall result reported in Sec. 2.4.2. According to eq. (11) the peeling force is $P_0/b = 0.03064\,\mathrm{N/m}$.

2. Peeling force for $EI = \infty$: If the bending stiffness is infinite, the strip does not deform and thus detaches at once from the substrate. Two boundary conditions are considered at $x = L$: (1) assuming fixed rotation and (2) assuming free rotation. In the first, case the strip remains parallel to the substrate during detachment and the maximum 'peeling force' is given by the maximum contact tension ($= -T_{\mathrm{min}}$) times the entire contact surface $L_{\mathrm{c}}b$, i.e.

$$P_{\infty,1} = -L_{\mathrm{c}} b T_{\mathrm{min}} \ , \tag{30}$$

where T_{min} denotes the minimum of T_{c} which is practically equal to the minimum of T given in eq. (16), i.e. $T_{\mathrm{min}} = -\sqrt{5}A_{\mathrm{H}}/(9\pi r_0^3)$. For $L_{\mathrm{c}} = 150\,\mathrm{nm}$, we thus find $P_{\infty,1}/b = 18.536\,\mathrm{N/m}$. The second case is more complicated to evaluate. During detachment, the rigid strip remains free to rotate. We suppose that the strip rotates about the bottom left corner point (at $x = 0$), denoted as $\mathcal{A}$ in the following. For a rotation of α, the moment balance around point $\mathcal{A}$ gives

$$P_{\infty,2}(\alpha) = -\frac{b}{L^*}\int_0^{L_{\mathrm{c}}\cos\alpha} \left(x_{\mathrm{c}} T_{\mathrm{c}} + M_{\mathrm{c}}\right) \mathrm{d}x \ , \tag{31}$$

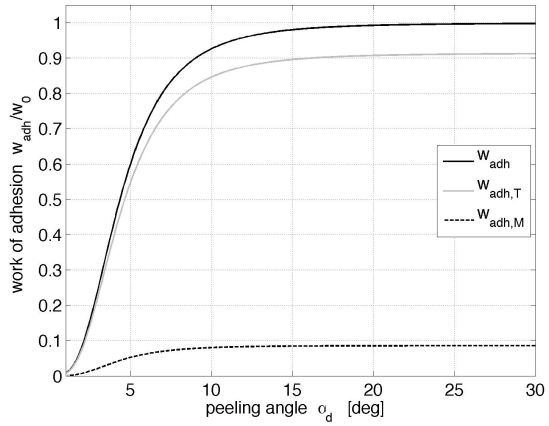

Figure 6: Influence of the peeling angle α_d on contributions $w_{\mathrm{adh,T}}$ and $w_{\mathrm{adh,M}}$. Saturation only occurs for large α_d.

where

$$\begin{aligned} L^* &= L\cos\alpha - h/2\sin\alpha \ , \\ x_{\mathrm{c}} &= x - h/2\sin\alpha \end{aligned} \tag{32}$$

denote the lever arms of forces P and T_{c} with respect to $\mathcal{A}$. T_{c} and M_{c} are given by eq. (15) and (23), setting

$$\begin{aligned} r_1 &= r_{\mathrm{eq}} + x\tan\alpha \ , \\ r_{\mathrm{M}} &= r_1 + h/2\cos\alpha \ , \\ r_2 &= r_1 + h\cos\alpha \ . \end{aligned} \tag{33}$$

Expression (31) can be evaluated numerically for various α. We thus find the maximum peeling force $\max(P_{\infty,2}/b) = 6.506\,\mathrm{N/m}$ at the angle $\alpha = \alpha_{\max} \approx 5.1 \cdot 10^{-4}$.[11]
It can be seen that the two limit cases, $EI = 0$ and $EI = \infty$, cover a large range of possible peeling forces so that intermediate models are needed to analyze the peeling behavior.

For finite values of the bending stiffness EI, a closed form solution cannot be obtained in general and the finite element method is therefore used to determine the peeling force. Fig. 7 shows the deformation of the peeling strip for different values of the applied displacement u. The strip parameters are taken as $E = 2\,\mathrm{GPa}$, $h = 10\,\mathrm{nm}$, $A_{\mathrm{H}} = 10^{-19}\,\mathrm{J}$ and $r_0 = 0.4\,\mathrm{nm}$ which corresponds to the values associated with gecko adhesion (Sauer, 2009). One can observe that, due to the finite bending stiffness, the strip axis is not parallel to the peeling direction. This property is one of the main differences to the Kendall result, where the force P remains parallel to the strip axis during peeling. In consequence, the peeling force increases significantly compared to the Kendall result.
This is shown in Fig. 8.a. Here, the force-displacement curve of the strip is displayed for different values of the bending stiffness EI, obtained by changing the stiffness E in multiples of $E_0 = 2\,\mathrm{GPa}$. For large EI, a distinct force maximum is observed whereas for low EI a long force plateau is observed. The latter case corresponds to the Kendall case and it can be seen that the Kendall result ($P/b = 30.64\,\mathrm{mN/m}$) is attained. For the gecko data ($E = E_0$), the maximum peeling force is nearly twice as large as the Kendall result, which shows that the Kendall result cannot be applied to the gecko spatula. The five dots on the $E = E_0$ curve correspond to the configurations shown in Fig. 7. Varying the stiffness E is analogous to varying the adhesion parameter A_{H} as Fig. 8.b shows. Changing E by a factor of γ corresponds to changing A_{H} by

[11] Due to the small angle we can approximate $\sin\alpha = \alpha$, $\cos\alpha = 1$, $L^* = L$ and $x_{\mathrm{c}} = x$ in eqs. (31)–(33).

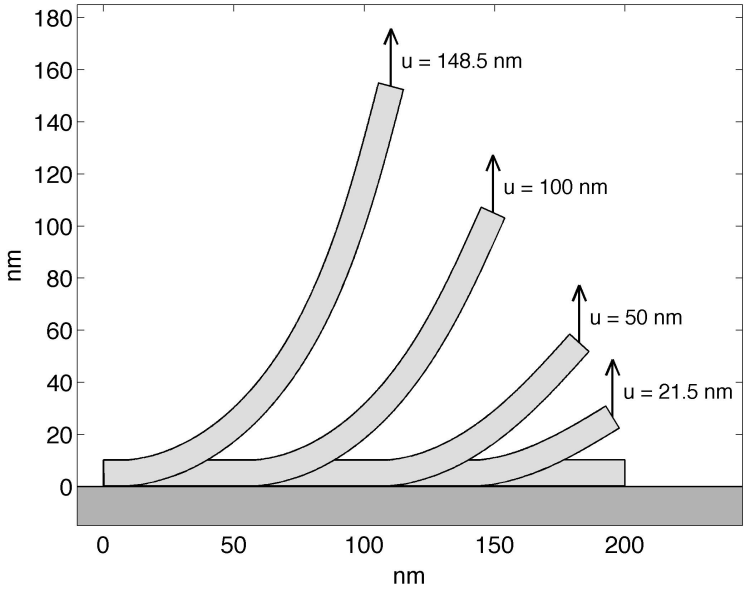

Figure 7: Strip deformation during peeling for the displacements $u = 0$, $u = 21.5\,\mathrm{nm}$ (which is the location of the maximum peeling force), $u = 50\,\mathrm{nm}$, $u = 100\,\mathrm{nm}$ and $u = 148.5\,\mathrm{nm}$. The strip parameters are taken as $E = 2\,\mathrm{GPa}$, $h = 10\,\mathrm{nm}$, $A_\mathrm{H} = 10^{-19}\,\mathrm{J}$ and $r_0 = 0.4\,\mathrm{nm}$.

$1/\gamma$. In Fig. 8.a the adhesion parameter is kept fixed at $A_\mathrm{H} = A_{\mathrm{H}0}$ while the stiffness is kept fixed at $E = E_0$ in Fig. 8.b. Note that changing E also affects the axial stiffness EA and the shear stiffness GA of the strip. The effect, however, is very weak so that the results in Fig. 8 change by less than a few per cent.

Changing the stiffness and the adhesion of the strip also affects the deformation. This is shown in Fig. 9, which considers the cases $E/A_\mathrm{H} = 10E_0/A_{\mathrm{H}0}$ (stiff strip with weak adhesion) and $A_\mathrm{H}/E = 10A_{\mathrm{H}0}/E_0$ (soft strip with strong adhesion). It can be seen that the strip deformation at the peeling zone cannot be approximated well by a curve with constant curvature, as is sometimes considered in the literature. The deformation states shown here are marked by dots in the corresponding force-displacement curves of Fig. 8.

Fig. 10 shows the dependance of the maximum peeling force on different values of EI. It can be seen that a smooth transition is obtained between the two limit cases discussed above: The Kendall limit ($P/b = 30.64\,\mathrm{mN/m}$) is reached from above, for stiffness values below $10^{-1}EI_0$, while the rigid limit is reached for stiffness values above $10^6 EI_0$. In fact, for the lowest stiffness considered ($EI = EI_0/30$) the maximum force is slightly lower than the Kendall result. This may be caused by the geometric nonlinearities of the numerical formulation. Note, that even though the results here are valid for general problem parameters, the actual force values depend on the specific geometry and material parameters of the strip. For the gecko spatula, the height varies roughly between $h = 10\,\mathrm{nm}$ at the pad to about $h = 100\,\mathrm{nm}$ at the shaft, so that we obtain the stiffness range indicated in the Fig. 10.[12]

As a final consideration, Table 1 examines the total peeling work, defined as the area under the peeling curve up to the stability point, i.e. the last data point of the force-displacement curves in Fig. 8, where the strip will snap into a new equilibrium configuration. At this point the strip may not be fully released, as Fig. 7 and 9 indicate, so that further work is required to

[12] In the computations, E is varied, while h is kept fixed. This does not correspond exactly to changing h for fixed E, due to the nonlinear influence of h in the contact formulation according to Sec. 3. Therefore the stiffness range of the spatula noted in Fig. 10 is only approximate.

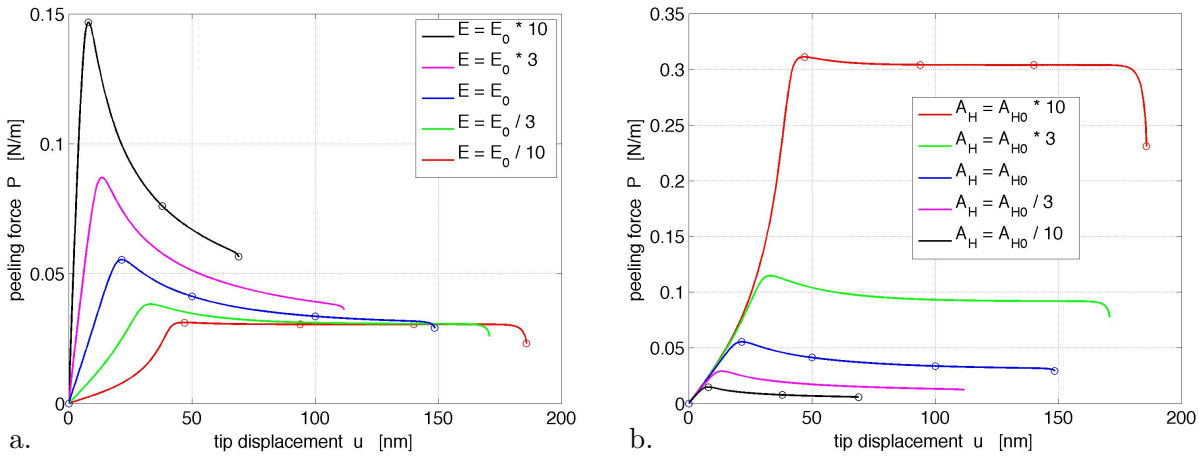

Figure 8: Force-displacement curve of the peeling strip for (a) different values of the stiffness E and (b) different values of the strength of adhesion A_{H}, both as multiples of the reference values $E_0 = 2\,\mathrm{GPa}$ and $A_{\mathrm{H0}} = 10^{-19}\,\mathrm{J}$. Curves with corresponding colors represent the same data.

E/E_0	Peeling work
0.1	4.785 nJ/m
0.3	5.022 nJ/m
1	5.403 nJ/m
3	5.720 nJ/m
10	5.813 nJ/m
10^2	5.564 nJ/m
10^3	4.819 nJ/m
10^4	3.510 nJ/m

Table 1: Total work required to peel off the elastic strip with $L = 200\,\mathrm{nm}$ and $h = 10\,\mathrm{nm}$ for different stiffness values E. A maximum is attained around $E = 10E_0$.

remove the strip. This additional work is not investigated here, since it will depend strongly on the exact boundary conditions and geometry at the tip of the strip. This is the reason why the peeling work can be lower than the limit value $w_{\mathrm{adh}}\, L_{\mathrm{c}} = 4.599\,\mathrm{nJ/m}$. Since energy is lost during snap-off and thus needs to be provided additionally, the peeling work can also be significantly larger than the limit value. For $EI = 10\,EI_0$, where the limit value is exceeded by 26.4%, the peeling work attains a maximum. Interestingly, this maximum falls into the stiffness range of the gecko spatula, which indicates that the spatula may represent an optimal design that tries to maximize the possible peeling energy.
For the finite element computations reported here, 300 two-node beam elements are used to discretize the strip and a displacement increment of $\Delta u = 0.25\,\mathrm{nm}$ is used to obtain dense output. Larger elements and load increments are possible if high order finite elements are used (Sauer, 2011).

5 Conclusion

This work discusses the peeling behavior of thin films with finite bending stiffness. The adhesion between film and substrate is modeled by the Lennard-Jones potential since it is suitable to describe van der Waals interaction, although the results and conclusions drawn here are also

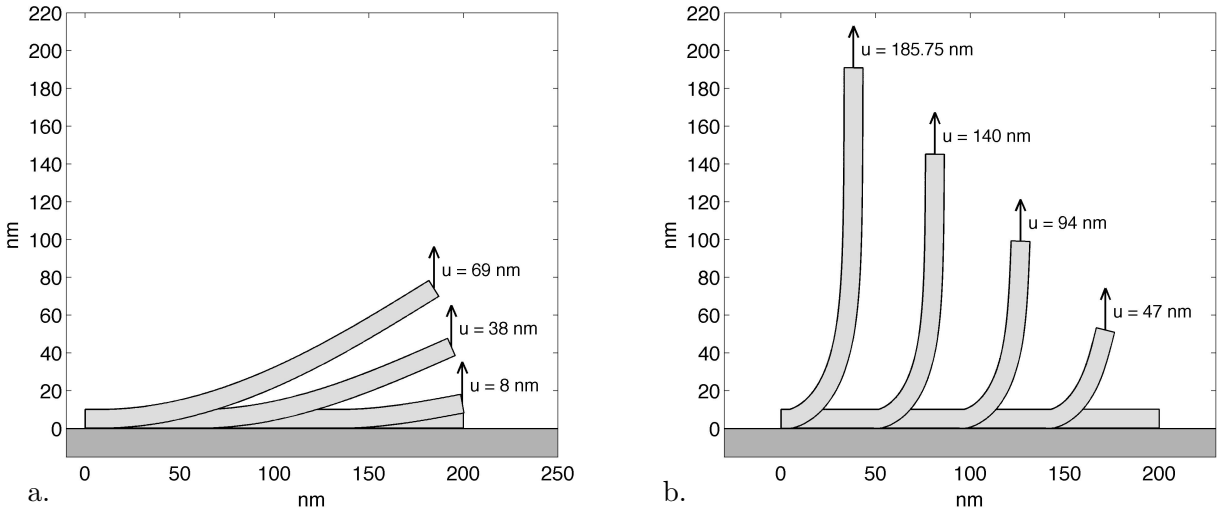

Figure 9: Peeling deformations of (a.) the stiff strip ($E/A_{\mathrm{H}} = 10E_0/A_{\mathrm{H0}}$) and (b.) the soft strip ($A_{\mathrm{H}}/E = 10A_{\mathrm{H0}}/E_0$).

valid for other cohesive zone models. Typically, only special cases can be solved by analytical methods. For example, if peeling is driven by pure bending, an analytical expression for the peeling moment can be found. For general loading conditions, which lead to combined bending, extension and shear deformations, numerical solution techniques, like the finite element method, need to be used. In this paper, a geometrically exact beam formulation is used to analyze the peeling behavior of thin films with finite bending stiffness, covering the entire range set by the limit cases for zero and infinite bending stiffness. The adhesion forces acting on the film lead to a distributed force and bending moment acting on the center axis of the beam. These also appear in the expression for the work of adhesion of the film. In the case of the gecko spatula, the bending stiffness is quite high and cannot be neglected, as is done when applying the Kendall peeling model. It is seen that the the spatula geometry maximizes the available peeling energy. Among future research steps is the inclusion of rate-dependant material response and frictional contact behavior due to the surface roughness at the substrate-film interface. Another useful extension is to develop a 3D beam formulation that accounts for torsion and skew bending and which is helpful to analyze complex peeling mechanisms occurring for narrow strips.

Acknowledgements

The author is grateful to the German Research Foundation (DFG) for supporting this research under project SA1822/5-1 and grant GSC 111.

References

Chen, B., Wu, P., and Gao, H. (2009). Pre-tension generates strongly reversible adhesion of a spatula pad on substrate. *J. R. Soc. Interface*, **6**(2065):529–537.

Gurtin, M. E. (1981). *An Introduction to Continuum Mechanics*. Academic Press.

Huber, G., Mantz, H., Spolenak, R., Mecke, K., Jacobs, K., Gorb, S. N., and Arzt, E. (2005). Evidence for capillarity contributions to gecko adhesion from single spatula nanomechanical measurements. *Proc. Natl. Acad. Sci. USA*, **102**(45):16293–16296.

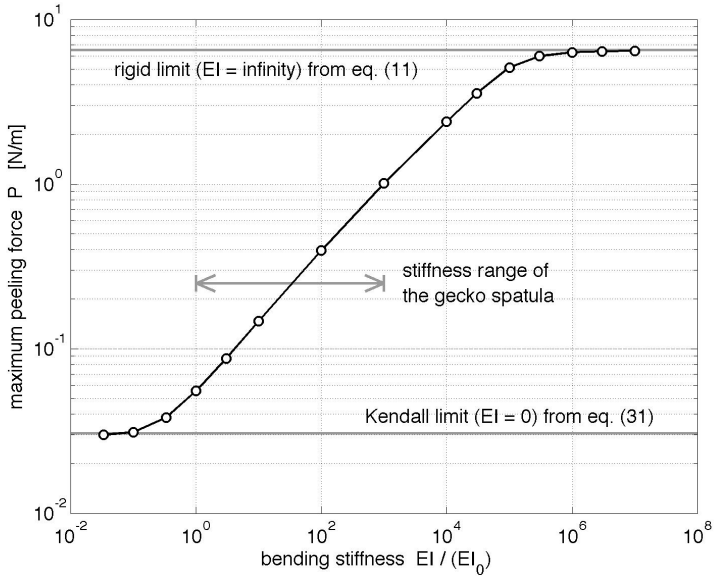

Figure 10: Maximum peeling force for different values of the bending stiffness EI. The approximate stiffness range of the gecko spatula is indicated.

Israelachvili, J. N. (1991). *Intermolecular and Surface Forces*. Academic Press, 2nd edition.

Kendall, K. (1975). Thin-film peeling – the elastic term. *J. Phys. D: Appl. Phys.*, **8**:1449–1452.

Li, S., Wang, J., and Thouless, M. D. (2004). The effects of shear on delamination in layered materials. *J. Mech. Phys. Solids*, **52**:193–214.

Molinari, A. and Ravichandran, G. (2008). Peeling of elastic tapes: Effects of large deformations, pre-straining, and of a peel-zone model. *J. Adhesion*, **84**:961–995.

Moore (Ed.), D. R. (2008). Special issue on peel testing. *Int. J. Adhesion Adhesives*, **28**:153–157.

Peng, Z. L., Chen, S. H., and Soh, A. K. (2010). Peeling behavior of a bio-inspired nano-film on a substrate. *Int. J. Solids. Struc.*, **47**:1952–1960.

Pesika, N. S., Tian, Y., Zhao, B., Rosenberg, K., Zeng, H., McGuiggan, P., Autumn, K., and Israelachvili, J. N. (2007). Peel-zone model of tape peeling based on the gecko adhesive system. *J. Adhesion*, **83**:383–401.

Sauer, R. A. (2009). Multiscale modeling and simulation of the deformation and adhesion of a single gecko seta. *Comp. Meth. Biomech. Biomed. Engng.*, **12**(6):627–640.

Sauer, R. A. (2011). Enriched contact finite elements for stable peeling computations. *Int. J. Numer. Meth. Engrg.*, **87**:593–616.

Sauer, R. A. and Li, S. (2007a). An atomic interaction-based continuum model for adhesive contact mechanics. *Finite Elem. Anal. Des.*, **43**(5):384–396.

Sauer, R. A. and Li, S. (2007b). A contact mechanics model for quasi-continua. *Int. J. Numer. Meth. Engrg.*, **71**(8):931–962.

Sauer, R. A. and Li, S. (2008). An atomistically enriched continuum model for nanoscale contact mechanics and its application to contact scaling. *J. Nanosci. Nanotech.*, **8**(7):3757–3773.

Sauer, R. A. and Wriggers, P. (2009). Formulation and analysis of a 3D finite element implementation for adhesive contact at the nanoscale. *Comput. Methods Appl. Mech. Engrg.*, **198**:3871–3883.

Thouless, M. D. and Yang, Q. D. (2008). A parametric study of the peel test. *Int. J. Adhesion Adhesives*, **28**:176–184.

Tian, Y., Pesika, N., Zeng, H., Rosenberg, K., Zhao, B., McGuiggan, P., Autumn, K., and Israelachvili, J. (2006). Adhesion and friction in gecko toe attachment and detachment. *Proc. Natl. Acad. Sci. USA*, **103**(51):19320–19325.

Williams, J. A. and Kauzlarich, J. J. (2005). The influence of peel angle on the mechanics of peeling flexible adherends with arbitrary load-extension characteristics. *Tribol. Int.*, **38**:951–958.

Williams, J. G. (1993). Root rotation an plastic work effects in the peel test. *J. Adhesion*, **41**:225–239.

Wriggers, P. (2006). *Computational Contact Mechanics*. Springer, 2nd edition.

Wriggers, P. (2008). *Nonlinear Finite Element Methods*. Springer.

Xu, X.-P. and Needleman, A. (1994). Numerical simulations of fast crack growth in brittle solids. *J. Mech. Phys. Solids*, **42**(9):1397–1434.